

Nitrogen Plasma Enhanced Low Temperature Atomic Layer Deposition of Magnesium Phosphorus Oxynitride (MgPON) Solid-State Electrolytes

Jin Su^{*ac}, Tohru Tsuruoka^{*a}, Takuji Tsujita^b, Yuu Inatomi^b, and Kazuya Terabe^a

a. International Center for Materials Nanoarchitectonics, National Institute for Materials Science, 1-1 Namiki, Tsukuba, Ibaraki 305-0044, Japan

b. Research and Development Center, Panasonic Energy Co. Ltd, Kadoma City, Osaka 571-8501, Japan

c. Current affiliation: Department of Materials, University of Oxford, Parks Road, Oxford, OX1 3PH, UK

*Corresponding Author: sujin23@outlook.com; TSURUOKA.Tohru@nims.go.jp

Abstract

Solid-state batteries (SSBs) that use solid electrolytes instead of flammable liquid electrolytes have the potential to generate higher specific capacity and offer better safety. Magnesium (Mg) based SSBs with Mg metal anodes are considered to be one of the most promising energy storage candidates, because it gives high theoretical volumetric capacities of 3830 mAh cm^{-3} . Here, we demonstrate an atomic layer deposition (ALD) process with a double nitrogen plasma process that successfully produces nitrogen-incorporated magnesium phosphorus oxynitride (MgPON) solid-state electrolyte (SSE) thin films at a low deposition temperature of 125°C . The ALD MgPON SSEs exhibit an ionic conductivity of 0.36 and $1.2 \mu\text{S cm}^{-1}$ at 450 and 500°C , respectively. The proposed ALD strategy shows the ability of conformal deposition nitrogen-doped SSEs on patterned substrates and is attractive for using nitride ion-conducting films as protective or wetting interlayers in solid-state Mg and Li batteries.

Introduction

Lithium (Li) ion batteries have been proven to be a highly efficient energy storage carrier due to their energy density, reliability, and rechargeability.¹⁻⁴ However, with the increasing requirement for higher energy and power density, conventional Li-ion batteries will encounter their limit.⁵⁻⁸ Magnesium (Mg) ion batteries with Mg metal anodes are considered to be one of the most promising energy storage candidates, because they give high theoretical volumetric (3830 mAh cm^{-3}) capacities, which are much greater than those achieved with Li anodes (2060 mAh cm^{-3}).⁹⁻¹¹ In addition, Mg metal is less air-sensitive than Li metal and has an insensitive dendrite formation nature, eliminating the safety issue of short circuits.⁹ Solid-state batteries (SSBs) that use solid-state electrolytes (SSEs) instead of flammable liquid electrolytes have the potential both to generate higher specific capacity and offer better safety,¹²⁻¹⁵ thus are being considered for widespread application in electric vehicles and the storage of electricity generated from intermittent renewable energy.¹⁶⁻¹⁸

Plenty of research has been explored the development of Mg-ion conducting SSEs, including hydrides,¹⁹ metal organic frameworks (MOFs),²⁰ and oxides,^{21,22} etc. Among these SSEs, ceramic oxides have attracted great interest because of their ease of material synthesis and high chemical and electrochemical stability.²¹⁻²³ Ikeda et al. synthesized a crystal $\text{Mg}_x\text{Zr}_y(\text{PO}_4)_z$ SSE material and obtained an ionic conductivity of $29 \mu\text{S cm}^{-1}$ at 400°C .²¹ Imanaka et al. reported a $\text{Mg}_x\text{Zr}_2\text{O}(\text{PO}_4)_2$ SSE composite that showed an ionic conductivity of 6.9 mS cm^{-1} at 800°C .²² Atomic layer deposition (ALD) is one of the most promising techniques for fabrication of SSEs, because it can provide dense and uniform solid

ion-conducting electrolyte films with precisely controlled thickness. This technique has also demonstrated to be able to achieve a high energy density in three-dimensionally (3D) structured thin-film SSBs with excellent conformality.²⁴⁻²⁹ Previously, we have reported that ALD magnesium phosphate (MgPO) SSE films with amorphous morphology show an Mg ionic conductivity of $0.16 \mu\text{S cm}^{-1}$ at 500°C .²⁴

Lithium phosphorus oxynitride (LiPON) with amorphous property has been able to achieve stable capacity retention over 10 000 cycles in a thin film battery with a lithium metal anode and a high-voltage lithium nickel manganese oxide cathode.³⁰ The most important feature of this LiPON thin-film is its homogeneous morphology without grain boundaries and porosity.³⁰⁻³² Nitrogen-doped LiPON thin-film shows a higher ionic conductivity and chemical stability than lithium phosphate.^{31, 32} Therefore, nitrogen doping is a viable way to improve the ionic conductivity and chemical stability of SSE films. Kozen et al. and Detavernier et al. reported that using nitrogen plasma during an ALD process is a possible way for nitrogen doping at a temperature above 250°C .^{33, 34} Unfortunately, during thin-film coating processes in an ALD chamber, high deposition temperatures above 250°C may cause some phase changes and decomposition for cathode and anode materials.³⁵ Even though a few reports showed that ammonia gas can be used as a nitrogen precursor for ALD nitrogen doping at low deposition temperatures. However, an indispensable ammonia scrubbing system would be used for vent gas disposal, which would significantly increase the cost of ALD equipment, maintenance difficulty, and safety issues. More importantly, a tiny amount of hyperactive ammonia gas remains in the ALD chamber, causing impurity of products.³⁶ Therefore, a nitrogen doping strategy for the ALD process at low deposition temperatures without using ammonia gas is highly required for thin-film nitrides coating on battery materials.

In this work, a plasma enhanced ALD system was used to fabricate magnesium phosphorus oxynitride (MgPON) thin films as Mg-ion conducting SSEs. This demonstrates that a proposed double nitrogen plasma process in ALD cycles plays an important role in nitrogen doping at a low deposition temperature of 125°C . The ALD MgPON SSE films exhibited amorphous nature and excellent conformal coverage on structured Si substrates. The ALD MgPON SSE film deposited at 125°C showed an Mg-ion conductivity of $1.2 \mu\text{S cm}^{-1}$ at 500°C , and the conductivity increased in a temperature range from 300 to 500°C with an activation energy of 1.60 eV . The observed ionic conductivity was significantly improved in nitrogen-incorporated MgPON SSEs, compared to the ALD MgPO film without nitrogen doping. These results demonstrate an encouraging nitrogen doping strategy that using a double nitrogen plasma process in one ALD cycle shows the ability of conformal deposition of nitride solid electrolytes onto 3D structured SSBs and is attractive for incorporating nitride thin-film SSEs into solid-state Mg and Li batteries.

Results and Discussion

A quaternary ALD process for MgPON SSE films was developed. A proposed schematic of ALD reaction steps for MgPON SSE deposition is illustrated in Figure 1. Bis(ethylcyclopentadienyl)magnesium ($\text{Mg}(\text{EtCp})_2$) and tris(dimethylamino)phosphine (TDMAP) precursors were used as magnesium and phosphorus sources, respectively. One ALD cycle started from a pulse introducing the TDMAP precursor onto an -OH groups terminated surface to form P-O bonds and dimethylamino phosphate ligands terminated surface, followed by an N_2 plasma pulse to provide nitrogen radicals and react with dimethylamino phosphate ligands for nitrogen incorporation. Another TDMAP precursor pulse was introduced to enhance the formation of P-N bonds. Then, an N_2+O_2 plasma pulse was applied to

provide nitrogen and oxygen radicals to remove dimethylamino phosphate ligands and form -OH groups simultaneously. The next step was a pulse introduction of the $\text{Mg}(\text{EtCp})_2$ precursor to react with -OH groups and form ethylcyclopentadienyl ligands terminated surface. Finally, an ALD cycle was completed by pulse introduction of H_2O to react with ethylcyclopentadienyl ligands forming Mg-OH groups on the surface. The ALD MgPON films can be fabricated to specific thicknesses by repeating these ALD cycles. For the N_2 plasma pulse, the carrier gas was completely replaced from Ar to N_2 to increase the nitrogen radicals. The central inset in Figure 1 is the proposed chemical structure of one ALD cycle deposition on the top surface of MgPON films. All the gas lines of the ALD system were held at 120°C to prevent condensation of precursors. The pulse times for TDMAP, N_2 plasma, N_2+O_2 plasma, and H_2O were taken for 3 s, while the pulse time for $\text{Mg}(\text{EtCp})_2$ was 4 s, followed by 20 s of Ar purge to remove residual precursors and oxidants. It can be emphasized that the proposed nitrogen doping strategy of using radio frequency nitrogen plasma twice as nitrogen precursor pulse-introducing process (we call 'double nitrogen plasma process') in one ALD cycle plays an important role in ALD nitrogen doping at low deposition temperatures.

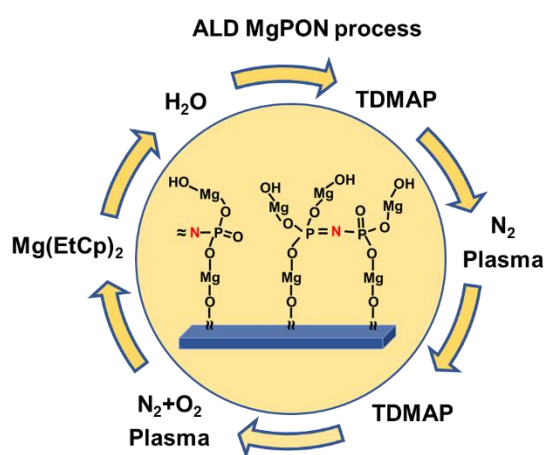


Figure 1. Schematic of proposed reaction steps in one cycle of ALD MgPON SSEs from TDMAP, N_2 plasma, N_2+O_2 plasma, $\text{Mg}(\text{EtCp})_2$, and H_2O precursors. The central inset illustrates the proposed chemical structure of one ALD cycle deposition on the top surface of MgPON SSE films. The symbol '≈' corresponds to omitted repetitive chemical groups.

The fabricated ALD MgPON films exhibited different growth rates depending on the deposition temperatures between 125 and 275°C , as shown in Figure 2a. The growth rate was relatively stable at around $3.0 \text{ \AA}/\text{cycle}$ at 125 and 175°C , but decreased to around $1.9 \text{ \AA}/\text{cycle}$ at 200 , 250 , and 275°C . Figures 2b represents Fourier transform infrared spectroscopy (FTIR) spectra measured for the films deposited at three deposition temperatures of 125 , 200 , and 250°C . Detailed comparisons for lower and higher deposition temperature are shown in Figure S1. The ALD MgPON film deposited at 125°C exhibited strong absorption peaks at 1648 and 1254 cm^{-1} , which are attributed to $\text{P}-\text{NP}_2$ and $\text{P}-\text{N}=\text{P}$ groups,³⁷ respectively. These peaks indicate that nitrogen was successfully incorporated into MgPON SSE films by our proposed ALD process. A small absorption peak at 805 cm^{-1} can be attributed to $\text{P}-\text{N}$ vibrations, also evidencing nitrogen incorporation. As the deposition temperature increased to 175°C , the absorption peak at 1648 cm^{-1} was slightly decreased. This suggests that the amount of the $\text{P}-\text{NP}_2$ unit was decreased, as shown in Figure S1. The clearly decreased intensity of this peak was observed for the film deposited at 200°C , as shown in Figure 2b, indicating further reduction of the

P-NP₂ units. This absorption peak disappeared at 250 °C or higher, indicating that the P-NP₂ bonds are not able to form at higher deposition temperatures. In contrast, the strong peak at 1254 cm⁻¹ was observed in all FTIR spectra. This suggests that nitrogen as a form of P-N=P can be incorporated in the MgPON films deposited at all deposition temperatures. The reduced growth rate at 200 °C or higher, as shown in Figure 2a, was consistent with the clearly decreased absorption peak intensity at 1648 cm⁻¹ (attributed to P-NP₂) and was evidence of the dramatically changed chemical bonds in ALD MgPON films. Absorption peaks at 1460 and 601 cm⁻¹ may suggest elongation of Mg-O-P bonds at lower deposition temperatures. On the other hand, absorption peaks at 1140 and 961 cm⁻¹ were observed at all deposition temperatures and can be attributed to asymmetric (ν_{as}) and symmetric (ν_s) stretching vibration of P-O and P-O-P linkages, respectively. From this analysis, we conclude that our proposed ALD process can incorporate nitrogen and successfully fabricate the MgPON SSE films. In particular, the ALD MgPON film deposited at 125 °C exhibited more diverse nitrogen-incorporated chemical bonds, resulting in disordering of the phosphate matrix. As a result, more space was created in the phosphate network at lower deposition temperatures. In contrast, the phosphate matrix was mainly composed of the P-NP₂ units at higher deposition temperatures, which makes the ALD MgPON films more packed, causing higher growth rates at lower deposition temperatures.

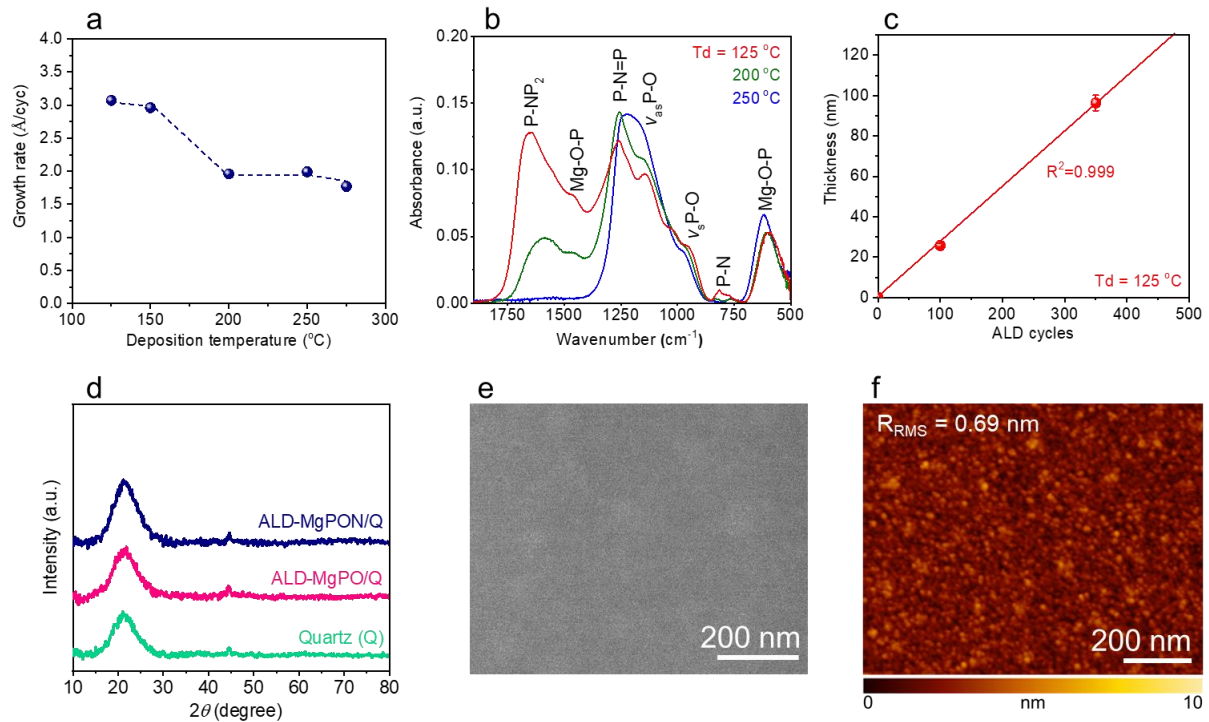


Figure 2. (a) Growth rates of ALD MgPON SSE films deposited at different temperatures. (b) FTIR spectra of MgPON films deposited at 125, 200, and 250 °C. (c) The thicknesses of ALD MgPON films are plotted as a function of the number of deposition cycles at 125 °C. The solid line was obtained via linear regression analysis, R^2 equal to 0.999. (d) XRD patterns of ALD MgPON and MgPO films deposited on quartz substrates at 125 °C. An XRD pattern of a quartz substrate is also shown as a reference. (e) SEM and (f) AFM images of the surface morphology of MgPON films deposited at 125 °C. The RMS roughness was estimated to be 0.69 nm.

The thicknesses of MgPON films deposited at 125 °C can be plotted linearly as a function of the number of ALD cycles, as shown in Figure 2c. The growth rate was calculated to be ≈ 3.0 Å/cycle at 125 °C up

to 350 cycles. The XRD pattern of an ALD MgPON film deposited on a quartz substrate did not exhibit any crystalline peaks, suggesting amorphous nature, as shown in Figure 2d. For comparison, diffraction patterns were obtained from our previously reported ALD MgPO films and a quartz substrate. This result indicates that the amorphous structure of the phosphate matrix is not affected by nitrogen doping. An SEM image of Figure 2e was obtained from the top surface of the ALD MgPON film deposited at 125 °C. The film exhibited a particularly smooth surface, which was also confirmed by an AFM image showing a root mean square (RMS) roughness of 0.69 nm, as shown in Figure 2f. As the deposition temperature increased to 250 °C, the surface of the MgPON film slightly changed and some smooth circles appeared, as shown in Figure S2a. It was confirmed that the AFM image exhibits a slightly increased RMS roughness of 2.2 nm, as shown in Figure S2b. This slight increase in surface roughness at higher deposition temperatures may arise from a slightly enhanced tendency toward crystallization, or increased precursor mobility and nucleation size, but the ALD MgPON film was still overall in the amorphous nature, as shown in Figure S3. It was concluded that ALD MgPON films deposited at all temperatures can provide extraordinarily uniform and smooth surfaces.

To investigate the chemical bonding states, X-ray photoemission spectroscopy (XPS) analyses were conducted on the surfaces of ALD MgPON and MgPO films deposited at 125 °C, as shown in Figure 3. The XPS peaks at binding energies of 531.2, 133.3, and 50.1 eV from the ALD MgPO film were assigned to O 1s, P 2p, and Mg 2p excitations, respectively, as shown in Figure 3a. In the survey XPS spectrum from the ALD MgPON film, except for those already existing O 1s, P 2p, and Mg 2p excitation peaks in the MgPO film, the appearance of the N 1s peak at 398.2 eV confirmed the incorporation of nitrogen in the film. The existence of the C 1s peak possibly came from incomplete surface reactions in the ALD processes or from ambient contamination on the surfaces during the transportation of the samples from the ALD chamber to the XPS apparatus. High-resolution XPS peaks fitting for O 1s, N 1s, P 2p, and Mg 2p regions from the surface of ALD MgPON and MgPO films are shown in Figures 3b-e and 3f-i, respectively. The O 1s spectrum consists of two peaks at 529.2 and 531.2 eV in both films, which were attributed to Mg-O and Mg-O-P bonds, respectively. The N 1s peak was observed only for the MgPON film and is deconvoluted into two peaks arising from the P-N=P group at 397.0 eV and the P-NP₂ group at 398.4 eV. A small peak was also observed at 402.3 eV, which may come from O=N-O units. The P 2p spectrum is composed of two peaks for the MgPON film, which are associated with P-N bonds at 130.1 eV and PO₄³⁻ units at 132.9 eV. Conversely, a single peak due to the PO₄³⁻ units was observed for the MgPO film. These fitted peaks in the N 1s and P 2p regions match well with those reported to identify the chemical characteristics of LiPON,^{29, 32} and also indicate that the nitrogen was successfully incorporated into the phosphate matrix by our proposed ALD process.

During XPS analyses, an Ar-ion depth profiling process was taken to investigate the depth dependence of the chemical bonding state of the ALD MgPON film. This Ar-ion beam etching process was performed at 1 eV for 3 min in a specific area. It was estimated to remove 12 nm thick film and create a new surface in the bulk film of the ALD MgPON SSE for XPS analyses. Figure S4 shows the survey and high-resolution XPS spectra measured for pristine and Ar-ion etched surfaces of an ALD MgPON film deposited at 125 °C. As shown in Figure S4a, the survey spectra exhibited all O 1s, N 1s, P 2p and Mg 2p excitation peaks in both pristine and Ar-ion etched surfaces, indicating that O, N, P, and Mg are homogeneously distributed over the entire ALD MgPON film. The Mg 2p region is assigned with the signal of Mg from MgPON. The O 1s peak at ≈532.1 eV of the pristine ALD MgPON, is attributed to the existence of O-C and O-H or P-O-P bonds on the film surface, as shown in Figure S4f. In addition to this, the absence of P-N=P peak at 397.0 eV and P-N peak at 130.1 eV possibly came from the

termination by H₂O precursor oxidizing the film surface to remove ethylcyclopentadienyl ligands in the final ALD process or from air contamination of the surface during the sample transportation.

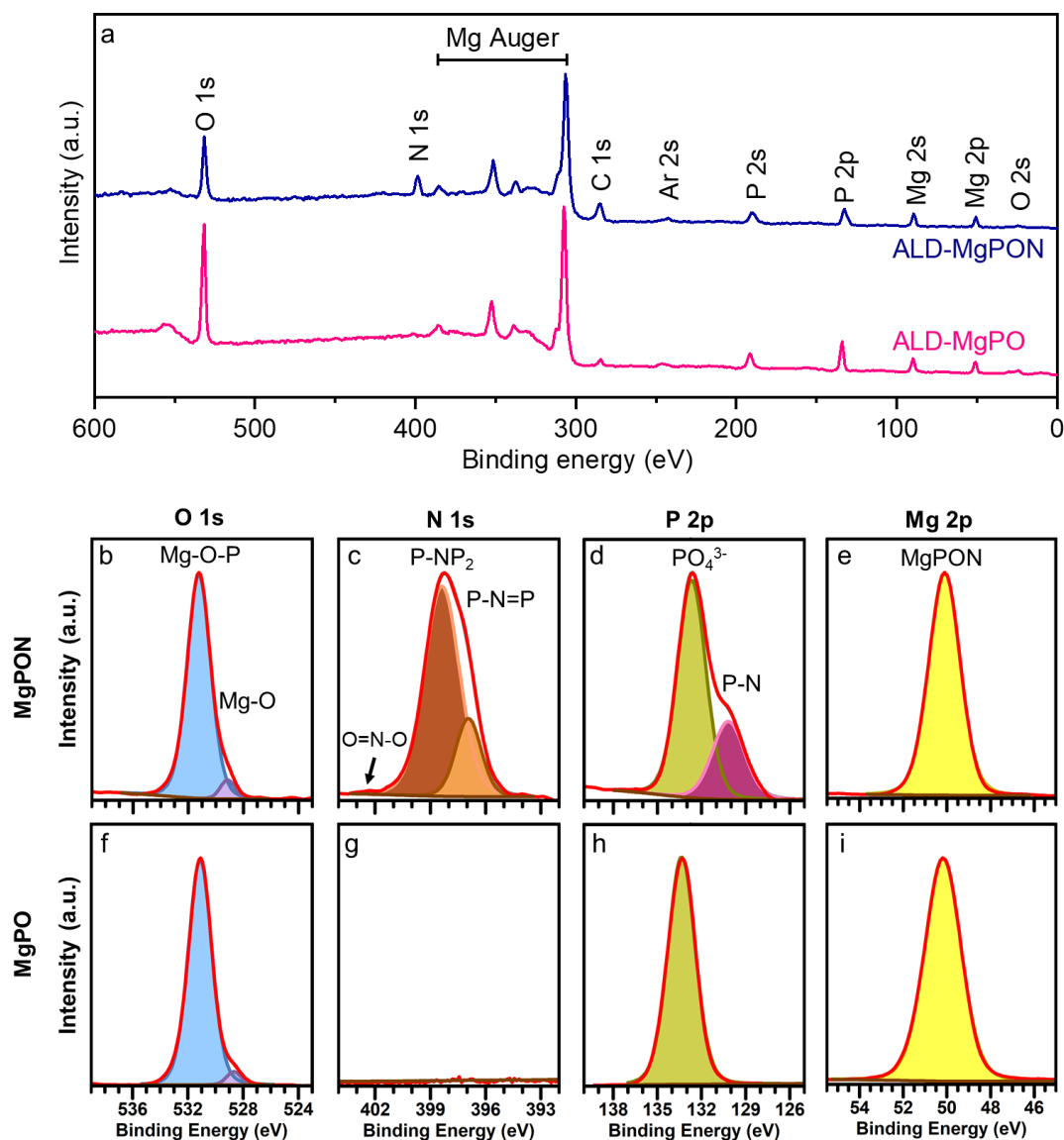


Figure 3. (a) Survey XPS spectra from the surface of ALD MgPON and MgPO SSE films deposited at 125 °C. High-resolution XPS spectra of ALD (b-e) MgPON and (f-i) MgPO films for O 1s, N 1s, P 2p, and Mg 2p regions. The Mg 2p region is assigned with the signal of Mg from MgPON.

XPS measurements were also carried out for ALD MgPON films deposited at 250 °C to investigate the temperature effect on the chemical bonding state. Figure S5a shows a comparison between survey and high-resolution XPS spectra measured for the ALD MgPON films deposited at 125 and 250 °C. The survey XPS spectra obtained from both films showed almost identical excitation peaks, demonstrating that nitrogen can be incorporated into MgPON films at all deposition temperatures examined. The P 2p spectra also evidence the nitrogen incorporation to form P–N bonds at all deposition temperatures. However, the N 1s spectra show that the chemical bonding state of the phosphate network is significantly different at different deposition temperatures. The ALD MgPON film deposited at 125 °C exhibited two peaks arising from P–N=P and P–NP₂ units, whereas the peak of P–NP₂ disappeared and only the peak of P–N=P was observed for the MgPON film deposited at 250 °C, as shown in Figure S5b-

i. This difference in chemical bonds for nitrogen is fully consistent with the FTIR results, where an absorption peak due to P-NP₂ units became smaller with increased deposition temperatures and disappeared at 250 °C, as shown in Figure 2b. The XPS and FTIR results indicate that the deposition temperature significantly influences the diversity of nitrogen-incorporated chemical bonds in the phosphate matrix, and lower deposition temperature is beneficial for more diverse nitrogen chemical bond incorporation in ALD MgPON SSE films. We also investigated the effect of N₂ flow rates on the N content in the ALD MgPON films during the N₂ plasma process. The chemical bonds and composition of those ALD MgPON films were measured by FTIR and XPS, as shown in Figures S6a and b. The FTIR results exhibited that the absorption peak corresponding to the P-N=P units was much higher than that of the P-NP₂ units at 20 SCCM while these peaks became comparable at 40 SCCM, as shown in Figure S6a. This suggests that the N₂ flow rate in the N₂ plasma has an impact on the chemical bonding states in the phosphate matrix. From the XPS survey spectra (as shown in Figure S6b), the relative elemental compositions were calculated to be Mg_{1.5}P₁O_{2.2}N_{0.40} and Mg_{1.3}P₁O_{1.3}N_{0.74} for 20 and 40 SCCM, respectively, as summarised in Table S1. This indicates that the N content of the ALD MgPON films can be adjusted by changing the N₂ flow rate during the N₂ plasma process.

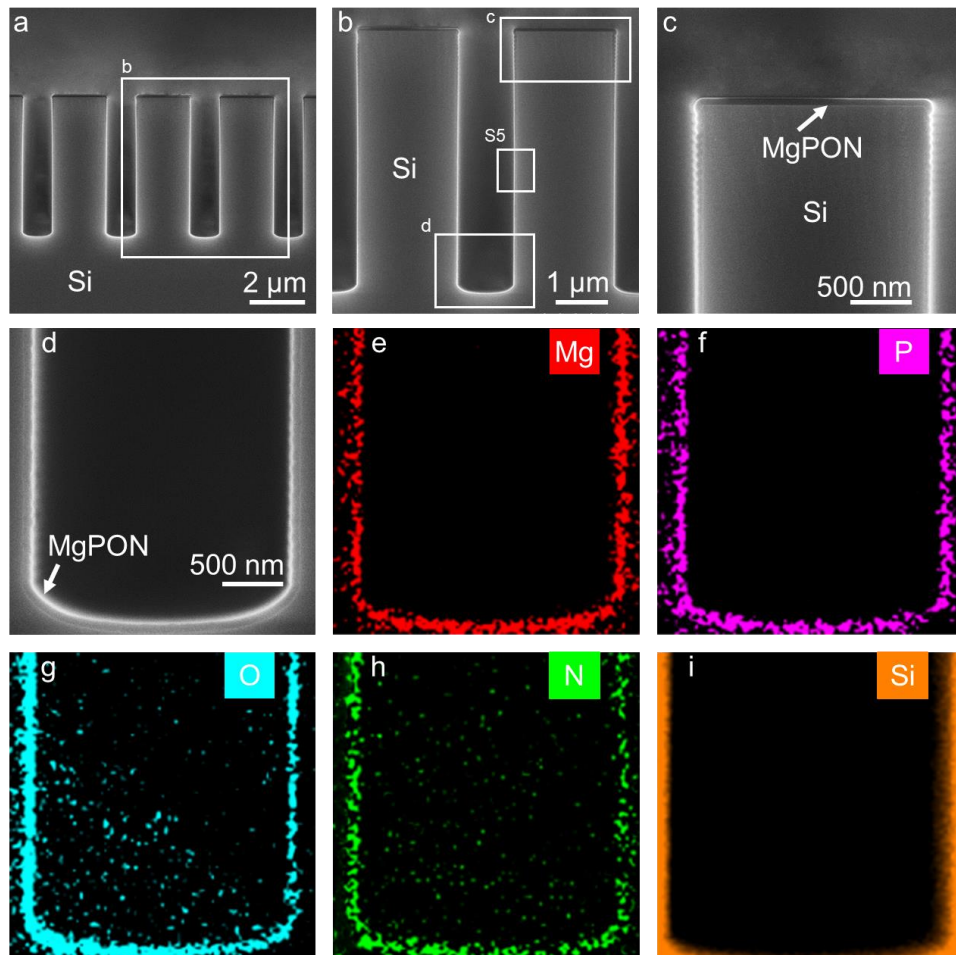


Figure 4. (a) Cross-sectional SEM images of the ALD MgPON SSE film deposited at 125 °C on a trench patterned Si substrate. Magnified views of (b) the trench structure, (c) the top, and (d) the bottom of the trench, with the corresponding (e-i) EDX mapping images for Mg, P, O, N, and Si.

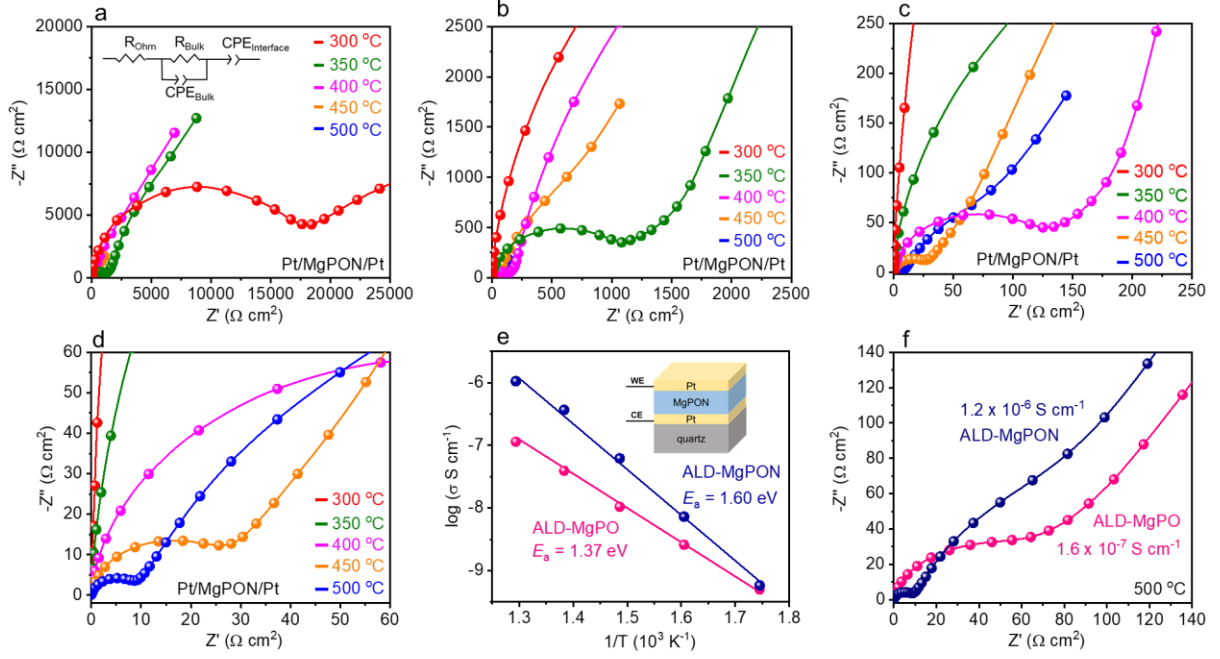


Figure 5. (a) EIS curves of a symmetric cell (Pt/MgPON/Pt) with an ALD MgPON SSE deposited at 125 °C, measured at ambient temperatures between 300 and 500 °C (the top inset illustrates the equivalent circuit model). (b-d) Magnified details of the Nyquist plots at different measurement temperatures. (e) The corresponding Arrhenius plot of the ionic conductivity. The top-right inset is a schematic illustration of the Pt/MgPON/Pt symmetric cell structure. (f) Comparison of typical EIS curves between the ALD MgPON and MgPO SSEs based symmetric cells measured at 500 °C.

To study the conformality and uniformity of the ALD MgPON SSE films, a Si substrate with a patterned trench structure was prepared by electron-beam lithography and reactive-ion etching to form trenches with a wide of 1.1 μm and a depth of 5 μm. An ALD MgPON film was deposited on this patterned Si substrate at 125 °C. A cross-sectional SEM image observed on this film is shown in Figure 4a. The magnified SEM images exhibit that the ALD MgPON film conformally and uniformly covered not only the top but also the sidewall and bottom of the trench structure, as shown in Figures 4b-d. The thickness of the film deposited on the bottom of the trench was estimated to be 62 nm, which is in good agreement with the thicknesses on the sidewall and top of the trench. In order to confirm the elemental homogeneity of the ALD MgPON film, EDX mapping was conducted on the cross-sectional area, as shown in Figure 4d. The resulting EDX images exhibited that Mg, P, O, and N are distributed uniformly at the bottom region of the trench, as shown in Figures 4e-i. The detailed SEM and EDX results from magnified sidewall were also obtained as shown in Figure S7, which further affirmed the uniformity of the ALD MgPON film. Therefore, we concluded that the proposed ALD MgPON process can deposit conformal and uniform SSE films on 3D patterned substrates with a high aspect ratio.

To characterize the ionic conductivity of the ALD MgPON films, electrochemical impedance spectroscopy (EIS) measurements were performed on cross-point structured symmetric cells consisting of a 93 nm thick ALD MgPON SSE film deposited at 125 °C with two Pt electrodes. The EIS profiles collected from a Pt/MgPON/Pt cell at ambient temperatures from 300 to 500 °C are presented in Figure 5a, and the magnified details of the Nyquist plots at different measurement temperatures are shown in Figure 5b-d. The upper-right inset in Figure 5e is a schematic illustration of the

Pt/MgPON/Pt cell. All resulting Nyquist plots from this Pt/MgPON/Pt cell exhibit semicircles at high frequency and spike tails at the low-frequency region, indicating typical ion-conducting behaviour. The semicircles at high frequencies correspond to the total resistance of the ALD MgPON film, while the tails at low frequencies are attributed to the polarization of the electrode-electrolyte interfaces, because of the capacitive behaviour of the blocking Pt electrodes. Such features are typically representative from the ionic conductivity measurement that is conducted for an ionic conductor with ion blocking electrodes.²⁴ The fitted curves for the EIS profiles were obtained using an equivalent circuit model (as shown in the top inset of Figure 5a). The equivalent circuit model is composed of three series units. The first unit is contact ohmic resistance (R_{ohm}), which is attributed to the high-frequency limiting resistance of the electrode. The second one consists of a parallel resistor (R_{Bulk}) and a constant-phase element (CPE_{Bulk}) corresponding to the bulk of the ALD MgPON film. The last component is another constant-phase element ($CPE_{interface}$) corresponding to the capacitive behaviour of the blocking Pt electrodes on the ALD MgPON SSE. The ALD MgPON films exhibited an amorphous nature, which has been confirmed by the XRD result, as shown in Figure 2d. Hence, it is rational to assume that the ALD MgPON films do not possess grain boundaries and is also consistent with the SEM images of Figures 2e and 4c,d. Therefore, it can be concluded that the measured bulk resistance is attributed only to the ALD MgPON SSE. The ionic conductivity σ of the ALD MgPON SSE can be calculated by $\sigma = d/(AR_{Bulk})$, where d is the thickness of the MgPON film and A is the geometric electrode area of the Pt/MgPON/Pt symmetric cell.

From the red colour Nyquist plot in Figure 5a, the bulk resistance R_{Bulk} of the ALD MgPON SSE was evaluated to be 16 k Ω cm² at 300 °C. It was decreased to 1.3 k Ω cm² as the ambient temperature increased to 350 °C, as shown in Figure 5b. The corresponding ionic conductivity was calculated to be 0.58 nS cm⁻¹ at 300 °C and it increased to 7.2 nS cm⁻¹ at 350 °C. As the ambient temperatures increased further to 400, 450, and 500 °C, the semicircles at high frequencies became diminishing, as shown in Figures 5c and 5d. The corresponding bulk resistance gradually decreased to 0.15 k Ω cm² at 400 °C, 26 Ω cm² at 450 °C, and 8.0 Ω cm² at 500 °C. As a result, the ionic conductivity for the ALD MgPON SSE was calculated to be 62 nS cm⁻¹, 0.36 μ S cm⁻¹, and 1.2 μ S cm⁻¹ at 400, 450, and 500 °C, respectively. The Arrhenius behaviour is plotted in Figure 5e, together with the result for the ALD MgPO film for comparison.²⁴ The activation energy of the ALD MgPON SSE was calculated to be 1.60 eV, which is slightly higher than the 1.37 eV of the ALD MgPO SSE. The ionic conductivity of the ALD MgPON SSE was 1.1 times higher than that of the ALD MgPO film at 300 °C. With increasing temperature, this difference in ionic conductivity becomes larger: 6.2 and 7.5 times at 400 and 500 °C, respectively. The Nyquist plots of the MgPON film exhibited significantly smaller semicircles than that of the MgPO film at 500 °C, as shown in Figure 5f, indicating the higher ionic conductivity of the ALD MgPON SSE (the comparisons of EIS plots at 300 and 400 °C are presented in Figure S8).

The thermal stability of both ALD MgPON and MgPO SSE films was also investigated by measuring the EIS profiles with an ambient temperature rise and drop cycle between 300 °C and 500 °C, as shown in Figure S9a. The ALD MgPO SSE film exhibited lowered ionic conductivity after the ambient temperature rose to 500 °C, and the conductivity decreased by more than one order of magnitude at 300 °C. The activation energy increased from 1.37 to 1.75 eV after ambient temperature rising to 500 °C. This reduced conductivity is attributed to the decomposition of the phosphate matrix by thermal desorption of P atoms at high temperatures (this result was reported in our previous works^{24, 38}). In contrast, the ALD MgPON SSE film showed almost unchanged ionic conductivity after the ambient temperature rose to 500 °C, which suggests that the nitrogen-incorporated ALD MgPON

SSE has higher thermal stability than the ALD MgPO SSE. From this electrochemical analysis, we conclude that the ALD MgPON SSE shows significantly increased ionic conductivity of $1.2 \mu\text{S cm}^{-1}$ at 500°C , compared with the ALD MgPO SSE, which has $0.16 \mu\text{S cm}^{-1}$ at 500°C . Our nitrogen doping process creates more diverse chemical bonds and reduces the interaction between cation and anion in the MgPON matrix, consequently, providing more space in the phosphate network as conduction pathways for Mg-ion migration. The evidence of the more diverse chemical bonds was confirmed by the appearance of P-N=P and P-NP₂ bonds from FTIR and XPS spectra (as shown in Figures **2b** and **3c**) for the ALD MgPON film deposited at 125°C .

As discussed above, deposition of the ALD MgPON film at different deposition temperatures resulted in different chemical bonding states. The ALD MgPON film deposited at 125°C contains P-N=P and P-NP₂ units, whereas the ALD MgPON film deposited at 250°C exhibited the absence of P-NP₂ units (as shown in Figures **2b** and S5f-i). This difference also affected the ionic conductivity. The comparison of the temperature variation of ionic conductivities between the ALD MgPON films deposited at 125°C and 250°C is represented in Figure S10. At an ambient temperature of 500°C , the ionic conductivity of the ALD MgPON film deposited at 250°C was $0.42 \mu\text{S cm}^{-1}$, which is 60 % lower than the ionic conductivity of the film deposited at 125°C . With decreasing ambient temperature, the ionic conductivity dropped steeply, and at 300°C , it was almost one order of magnitude lower than the ionic conductivity of the ALD MgPON film deposited at 125°C . The activation energy was calculated to be 1.66 eV, which is slightly higher than that of the ALD MgPON film deposited at 125°C . This reduced ionic conductivity of the ALD MgPON film deposited at 250°C can be attributed to the absence of P-NP₂ units in MgPON films. The reduction of P-NP₂ units results in a monophasic phosphate network that may suppress the Mg-ion mobility in the ALD MgPON SSE. Therefore, it can be concluded that lower deposition temperatures play an important role in improving the ionic conductivity of the ALD MgPON SSE film. The ionic conductivity of the ALD MgPON films with different N₂ flow rates during the N₂ plasma process was also investigated, as shown in Figure S11. The ionic conductivity of the film deposited with 20 SCCM N₂ flow rate was distinctly lower than that of the film deposited with 40 SCCM. The corresponding activation energy was 1.64 eV for 20 SCCM, which was slightly higher than 1.60 eV for 40 SCCM. This reduced conductivity of the ALD MgPON film deposited with the lower N₂ flow rate can be attributed to the decreased N content as well as the reduced amount of P-NP₂ unit in the MgPON film, as shown in S6a and b. Our results illustrate that the encouraging strategy of using a double nitrogen plasma process in the ALD cycles has great potential to overcome some of the primary challenges for ALD nitrogen doping, and will be able to produce not only Mg-based but also Li-based ion-conducting SSEs with high stability.

Conclusion

We have demonstrated that a new plasma enhanced ALD process successfully incorporated nitrogen into MgPON SSE thin films using TDMAP, Mg(EtCp)₂, N₂ plasma, N₂+O₂ plasma, and H₂O precursors. The ALD MgPON SSEs deposited at 125°C showed an amorphous nature without grain boundaries and exhibited an ionic conductivity of $0.36 \mu\text{S cm}^{-1}$ and $1.2 \mu\text{S cm}^{-1}$ at ambient temperatures of 450°C and 500°C , respectively. The resultant ionic conductivity showed an Arrhenius behaviour with an activation energy of 1.60 eV for the ALD MgPON SSE film deposited at 125°C . The obtained ionic conductivity for this ALD MgPON SSE film is 7.5 times higher than that of the ALD MgPO film ($0.16 \mu\text{S cm}^{-1}$) at 500°C . The chemical bonds of incorporated nitrogen can introduce more covalent bonds of P-N, which lower the electrostatic Mg-O binding and provide more space and pathway in the

phosphate network for more efficient Mg-ion migration. It was also found that the incorporated nitrogen improves the thermal stability of the ALD MgPON film compared to the ALD MgPO film. The ALD MgPON films deposited at lower temperatures exhibited more diversity of nitrogen incorporated phosphate matrix including P-N=P and P-NP₂ units, while the films deposited at 250 °C or higher showed clearly an absence of nitrogen bonded of P-NP₂ units. As a result, the ALD MgPON films deposited at 125 °C presented a higher ionic conductivity than those films deposited at higher temperatures, suggesting the importance of the deposition temperature to control the chemical bonding state of the phosphate matrix during the ALD process. These results demonstrate that our proposed ALD MgPON strategy with a double nitrogen plasma process in ALD cycles plays an important role in ALD nitrogen doping at low deposition temperatures. It also showed the capability of conformal deposition of nitride solid electrolytes onto 3D nanostructures with a high aspect ratio. We believe that our proposed ALD strategy can overcome the primary challenge for low-temperature ALD nitrogen doping and produce uniform and conformal nitrogen-incorporated SSEs. This technique can be applied to other types of ALD nitride materials and is very encouraging and desirable for incorporating nitride thin-film SSEs as separators, protective or wetting interlayers into solid-state magnesium and lithium batteries.

Experimental Details

Preparation and growth conditions of ALD MgPON SSE films

ALD MgPON films were deposited on a variety of substrates, which includes Si, SiO₂-covered Si, Pt-coated Si, and Pt-coated quartz. All substrates were cleaned by ultrasonication in acetone and ethanol solvent for 10 min, followed by plasma surface cleaning in the O₂ atmosphere, then transferred to a plasma-enhanced ALD system (SPLEAD Co. Ltd.). The ALD MgPON films were fabricated using tris(dimethylamino)phosphine (TDMAP), bis(ethylcyclopentadienyl)magnesium (Mg(EtCp)₂) as precursor gas and H₂O as oxidant gas under a base pressure of 10⁻³ Pa. A process pressure was maintained at ~40 Pa via Ar gas flow with 40 SCCM, and the deposition temperatures were varied from 125 °C to 275 °C. All precursors were delivered to the deposition chamber via a 10 SCCM Ar carrier gas. The N₂ plasma and N₂+O₂ plasma were produced by a radio frequency plasma configuration, in which a voltage was applied between a showerhead and a substrate holder. The radio frequency power was set at 100 W for the N₂ plasma and 50 W for the N₂+O₂ plasma. For the N₂ plasma process, the Ar carrier gas was replaced with N₂ gas via flow rates of 20-40 SCCM.

Characterization

The growth rates of the ALD MgPON films deposited on SiO₂-covered Si substrates were measured using a J. A. Woollam M-2000 and EC-400 spectroscopic ellipsometer from the wavelength region of 400-1000 nm. Fourier transform infrared spectroscopy (FTIR) was applied to analyze the chemical bonding states of the ALD MgPON films deposited on Pt-covered Si substrates. The FTIR measurements were performed in an attenuated total reflectance mode (ATR) using a Thermo Fisher Nicolet 4700 spectrometer over the wavenumber region of 500-4000 cm⁻¹. X-ray photoelectron spectroscopy (XPS, PHI Quantera) was used to analyze chemical bonding states on the surface of ALD MgPON SSE films. Survey and specific high-resolution spectra were collected using a monochromatic Al Kα X-ray source. The binding energy of 284.8 eV (C 1s) was used for energy calibration. The XPS results were analyzed using CasaXPS software for peak fitting and chemical bond ascription. The surface morphology of the ALD MgPON films deposited on SiO₂-covered Si substrates was

characterized by atomic force microscopy (AFM, SII E-Sweep/Nano Navi II) at a scan rate of 1 Hz. X-ray diffraction (XRD) was applied to confirm the crystallinity of the ALD MgPON films deposited on quartz substrates using a Rigaku SmartLab X-ray diffractometer with Cu K α_1 radiation. Scanning electron microscopy (SEM) images were collected to confirm the morphology and structure of ALD MgPON films deposited on Si substrates using a Hitachi SU8230 SEM system with an acceleration voltage of 10 kV. Energy-dispersive X-ray spectroscopy (EDX) scans were conducted to collect the elemental mapping.

Symmetric cell assembly and electrochemical characterization

ALD MgPON SSE films with a thickness of ~ 100 nm were deposited on Pt-coated quartz substrates by the plasma-enhanced ALD system. 100 nm thick Pt electrodes were deposited on the surface of ALD MgPON films by using radio frequency magnetron sputtering under a pressure of 0.43 Pa with a powder density of 2.4 W cm^{-2} using a metal mask, to form Pt/MgPON/Pt symmetric cells with a junction area of $0.2 \times 0.2 \text{ mm}^2$ for Mg ionic conductivity measurements. Electrochemical impedance spectroscopy (EIS) measurements were conducted on these Pt/MgPON/Pt symmetric cells using a Solartron 1260 analyzer with a 1296 dielectric interface over a frequency range from 1 MHz to 100 mHz, with a perturbation amplitude of 5 mV in an Ar-filled glovebox ($\text{O}_2 < 0.2 \text{ ppm}$). During the EIS measurements, the ambient temperature was controlled from 300 to 500 °C. The EIS data were analyzed using the ZView software.

Author Contributions

J. S. and T. Tsuruoka conceived the idea of the ALD MgPON SSE process. T. Tsuruoka and K. T. supervised the project. J. S. prepared the ALD samples and conducted the FTIR, XRD, SEM, EDX, ellipsometry characterizations, and electrochemical experiments. T. Tsujita performed XPS measurements. J. S. and T. Tsuruoka interpreted the data and wrote the manuscript with contributions from all authors.

Acknowledgments

This work was supported by the Panasonic-NIMS Center of Excellence for Advanced Functional Materials and the JSAP KAKENHI Grant Number 21H03412.

Conflict of interest

The authors declare no conflict of interest.

Data Availability Statement

The data that support the findings of this study are available from the corresponding author upon reasonable request.

References

- [1] B. Dunn, H. Kamath, J. M. Tarascon, *Science* 2011, 334, 928-935.

- [2] W. Xu, J. L. Wang, F. Ding, X. L. Chen, E. Nasybutin, Y. H. Zhang, J. G. Zhang, *Energy & Environmental Science* **2014**, 7, 513-537.
- [3] D. Larcher, J. M. Tarascon, *Nature Chemistry* **2015**, 7, 19-29.
- [4] G. M. Hobold, J. Lopez, R. Guo, N. Minafra, A. Banerjee, Y. S. Meng, Y. Shao-Horn, B. M. Gallant, *Nature Energy* **2021**, 6, 951-960.
- [5] M. R. Palacin, A. de Guibert, *Science* **2016**, 351, 6273.
- [6] Y. M. Chen, Z. Q. Wang, X. Y. Li, X. H. Yao, C. Wang, Y. T. Li, W. J. Xue, D. W. Yu, S. Y. Kim, F. Yang, A. Kushima, G. G. Zhang, H. T. Huang, N. Wu, Y. W. Mai, J. B. Goodenough, J. Li, *Nature* **2020**, 578, 251-255.
- [7] J. Deng, C. Bae, A. Denlinger, T. Miller, *Joule* **2020**, 4, 511-515.
- [8] P. G. Bruce, B. Scrosati, J. M. Tarascon, *Angewandte Chemie-International Edition* **2008**, 47, 2930-2946.
- [9] J. Muldoon, C. B. Bucur, T. Gregory, *Chemical Reviews* **2014**, 114, 11683-11720.
- [10] H. D. Yoo, I. Shterenberg, Y. Gofer, G. Gershinsky, N. Pour, D. Aurbach, *Energy & Environmental Science* **2013**, 6, 2265-2279.
- [11] T. Gao, F. D. Han, Y. J. Zhu, L. M. Suo, C. Luo, K. Xu, C. S. Wang, *Advanced Energy Materials* **2015**, 5, 1401507.
- [12] Y. G. Lee, S. Fujiki, C. Jung, N. Suzuki, N. Yashiro, R. Omoda, D. S. Ko, T. Shiratsuchi, T. Sugimoto, S. Ryu, J. H. Ku, T. Watanabe, Y. Park, Y. Aihara, D. Im, I. T. Han, *Nature Energy* **2020**, 5, 299-308.
- [13] J. Janek, W. G. Zeier, *Nature Energy* **2016**, 1, 16141.
- [14] J. Su, M. Pasta, Z. Y. Ning, X. W. Gao, P. G. Bruce, C. R. M. Grovenor, *Energy & Environmental Science* **2022**, 15, 3805-3814.
- [15] R. S. Chen, Q. H. Li, X. Q. Yu, L. Q. Chen, H. Li, *Chemical Reviews* **2020**, 120, 6820-6877.
- [16] J. B. Goodenough, *Energy & Environmental Science* **2014**, 7, 14-18.
- [17] J. Su, T. Hisatomi, T. Minegishi, K. Domen, *Angewandte Chemie-International Edition* **2020**, 59, 13800-13806.
- [18] S. Chu, A. Majumdar, *Nature* **2012**, 488, 294-303.
- [19] R. Le Ruyet, B. Fleutot, R. Berthelot, Y. Benabed, G. Hautier, Y. Filinchuk, R. Janot, *Acs Applied Energy Materials* **2020**, 3, 6093-6097.
- [20] M. L. Aubrey, R. Ameloot, B. M. Wiers, J. R. Long, *Energy & Environmental Science* **2014**, 7, 667-671.
- [21] S. Ikeda, M. Takahashi, J. Ishikawa, K. Ito, *Solid State Ionics* **1987**, 23, 125-129.
- [22] N. Imanaka, Y. Okazaki, G. Adachi, *Journal of Materials Chemistry* **2000**, 10, 1431-1435.
- [23] Q. Zhao, S. Stalin, C. Z. Zhao, L. A. Archer, *Nature Reviews Materials* **2020**, 5, 229-252.
- [24] J. Su, T. Tsuruoka, T. Tsujita, Y. Nishitani, K. Nakura, K. Terabe, *Chemistry of Materials* **2019**, 31, 5566-5575.

- [25] Y. Zhao, L. Zhang, J. Liu, K. Adair, F. P. Zhao, Y. P. Sun, T. P. Wu, X. X. Bi, K. Amine, J. Lu, X. L. Sun, *Chemical Society Reviews* **2021**, *50*, 3889-3956.
- [26] M. Nisula, Y. Shindo, H. Koga, M. Karppinen, *Chemistry of Materials* **2015**, *27*, 6987-6993.
- [27] Y. C. Perng, J. Cho, S. Y. Sun, D. Membreno, N. Cirigliano, B. Dunn, J. P. Chang, *Journal of Materials Chemistry A* **2014**, *2*, 9566-9573.
- [28] E. Kazyak, K. H. Chen, K. N. Wood, A. L. Davis, T. Thompson, A. R. Bielinski, A. J. Sanchez, X. Wang, C. M. Wane, J. Sakamoto, N. P. Dasgupta, *Chemistry of Materials* **2017**, *29*, 3785-3792.
- [29] A. J. Pearse, T. E. Schmitt, E. J. Fuller, F. El-Gabaly, C. F. Lin, K. Gerasopoulos, A. C. Kozen, A. A. Talin, G. Rubloff, K. E. Gregorczyk, *Chemistry of Materials* **2017**, *29*, 3740-3753.
- [30] J. C. Li, C. Ma, M. F. Chi, C. D. Liang, N. J. Dudney, *Advanced Energy Materials* **2015**, *5*, 1401408.
- [31] J. B. Bates, N. J. Dudney, B. Neudecker, A. Ueda, C. D. Evans, *Solid State Ionics* **2000**, *135*, 33-45.
- [32] Y. Su, J. Falgenhauer, A. Polity, T. Leichtweiss, A. Kronenberger, J. Obel, S. Zhou, D. Schlettwein, J. Janek, B. K. Meyer, *Solid State Ionics* **2015**, *282*, 63-69.
- [33] A. C. Kozen, A. J. Pearse, C. F. Lin, M. Noked, G. W. Rubloff, *Chemistry of Materials* **2015**, *27*, 5324-5331.
- [34] L. Henderick, H. Hamed, F. Mattelaer, M. Minjauw, J. Meersschant, J. Dendooven, M. Safari, P. Vereecken, C. Detavernier, *Acs Applied Materials & Interfaces* **2020**, *12*, 25949-25960.
- [35] Y. Huang, Y. C. Lin, D. M. Jenkins, N. A. Chernova, Y. Chung, B. Radhakrishnan, I. H. Chu, J. Fang, Q. Wang, F. Omenya, S. P. Ong, M. S. Whittingham, *Acs Applied Materials & Interfaces* **2016**, *8*, 7013-7021.
- [36] M. Z. Ansari, D. K. Nandi, P. Janicek, S. A. Ansari, R. Ramesh, T. Cheon, B. Shong, S. H. Kim, *Acs Appl Mater Inter* **2019**, *11*, 43608-43621.
- [37] G. Socrates, G. Socrates, *Infrared and Raman characteristic group frequencies : tables and charts*, 3rd ed., Wiley, Chichester ; New York, **2001**.
- [38] T. Tsuruoka, T. Tsujita, J. Su, Y. Nishitani, T. Hamamura, Y. Inatomi, K. Nakura, K. Terabe, *Japanese Journal of Applied Physics* **2020**, *59*, SIIG08.

Supplementary Information

Nitrogen Plasma Enhanced Low Temperature Atomic Layer Deposition of Magnesium Phosphorus Oxynitride (MgPON) Solid-State Electrolytes

Jin Su^{*ac}, Tohru Tsuruoka^{*a}, Takuji Tsujita^b, Yuu Inatomi^b, and Kazuya Terabe^a

a. International Center for Materials Nanoarchitectonics, National Institute for Materials Science, 1-1 Namiki, Tsukuba, Ibaraki 305-0044, Japan

b. Research and Development Center, Panasonic Energy Co. Ltd, Kadoma City, Osaka 571-8501, Japan

c. Current affiliation: Department of Materials, University of Oxford, Parks Road, Oxford, OX1 3PH, UK

Corresponding Authors

*E-mail: sujin23@outlook.com; TSURUOKA.Tohru@nims.go.jp

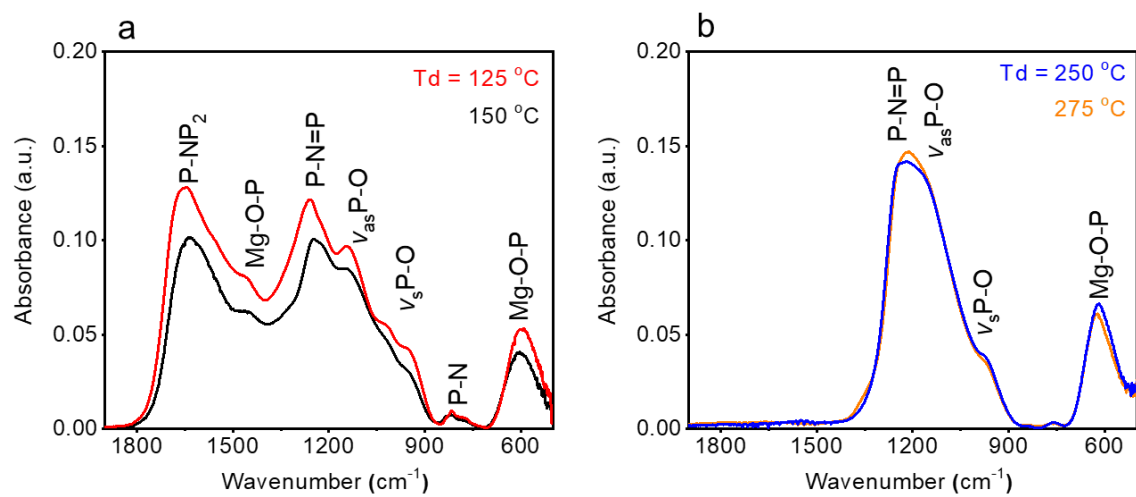


Figure S1. FTIR spectra of ALD MgPON films deposited at (a) lower deposition temperatures (T_d) of 125 and 150 $^\circ\text{C}$ and (b) higher deposition temperatures of 250 and 275 $^\circ\text{C}$.

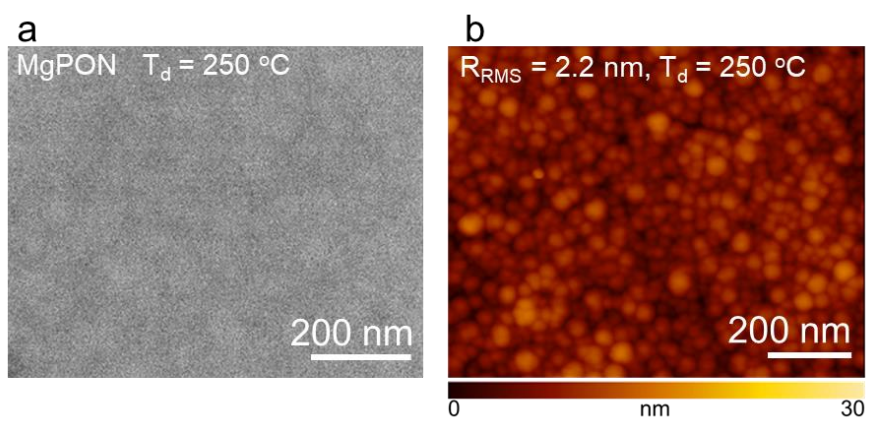


Figure S2. (a) SEM and (b) AFM images of the surface morphology of an ALD MgPON film deposited at 250 °C. The RMS roughness was estimated to be 2.2 nm.

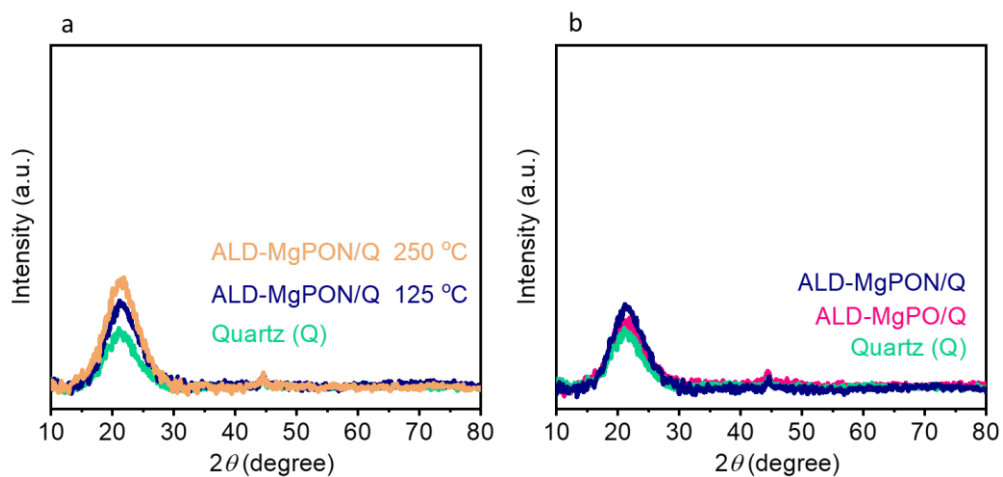


Figure S3. (a) XRD patterns of ALD MgPON films deposited at 125 and 250 °C on quartz substrates. An XRD pattern of a quartz substrate is also shown as a reference. (b) XRD patterns of ALD MgPON and MgPO films deposited on quartz substrates at 125 °C (normalized XRD patterns from Figure 2d to one baseline). The ALD MgPON and MgPO films showed increased peak intensities at 22°, which may come from slightly enhanced tendency toward crystallization although they still maintained overall amorphous nature.

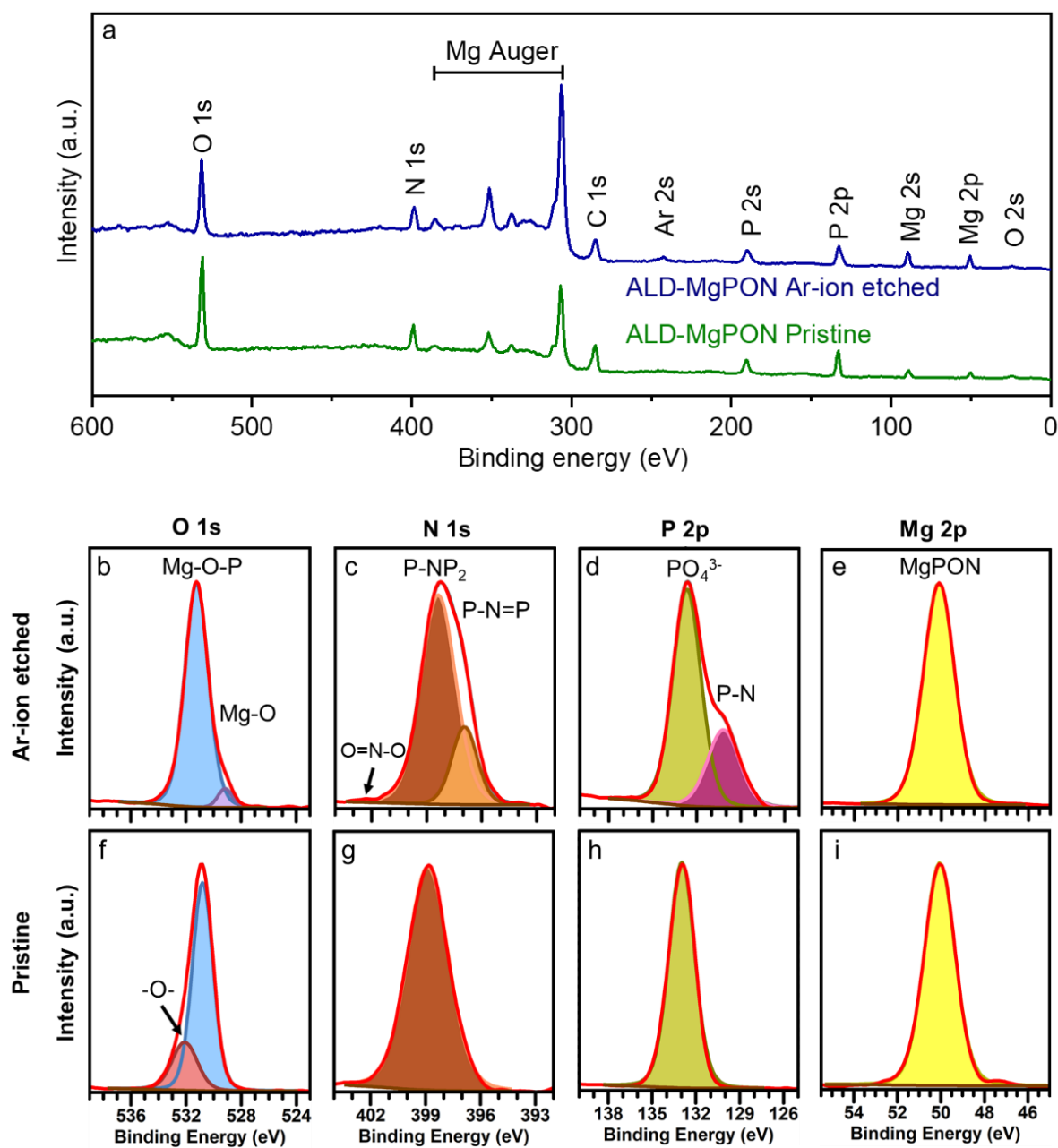


Figure S4. (a) Survey XPS spectra from the pristine and Ar-ion etched (1 keV for 3 min) surfaces of an ALD MgPON film deposited at 125 °C. High-resolution XPS spectra of (b-e) Ar-ion sputtered and (f-i) pristine surfaces of an ALD MgPON film, measured for O 1s, N 1s, P 2p and Mg 2p regions with fitted curves. “-O-” corresponds to the peak at ~532.1 eV from the existence of O-C and O-H or P-O-P bonds on the ALD MgPON film surface. The Mg 2p region is assigned with the signal of Mg from MgPON.

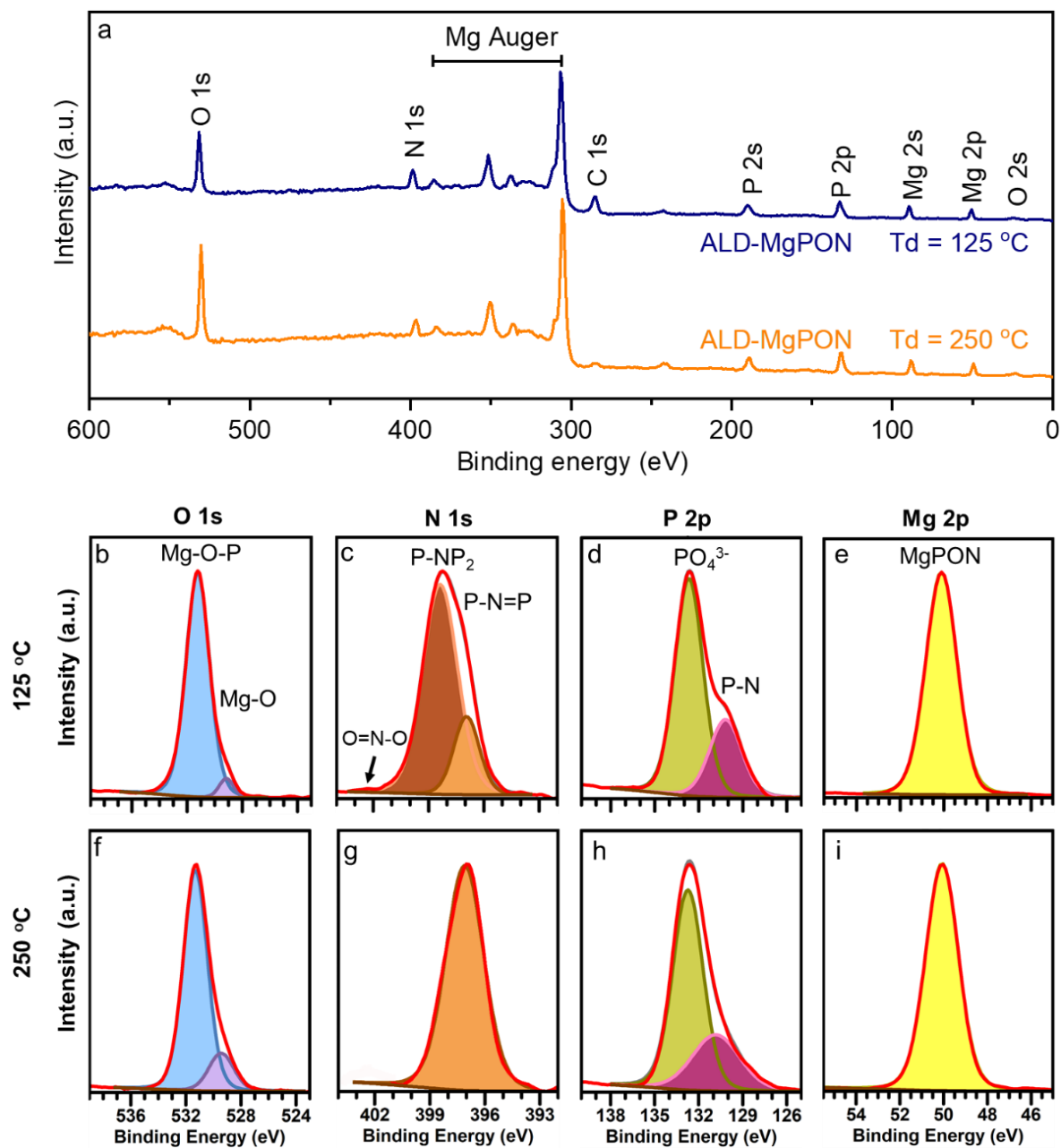


Figure S5. (a) Survey XPS spectra from ALD MgPON films deposited at 125 and 250 °C. High-resolution XPS spectra of O 1s, N 1s, P 2p and Mg 2p regions, measured for the film deposited at (b-e) 125 °C and (f-i) 250 °C, respectively. The Mg 2p region is assigned with the signal of Mg from MgPON.

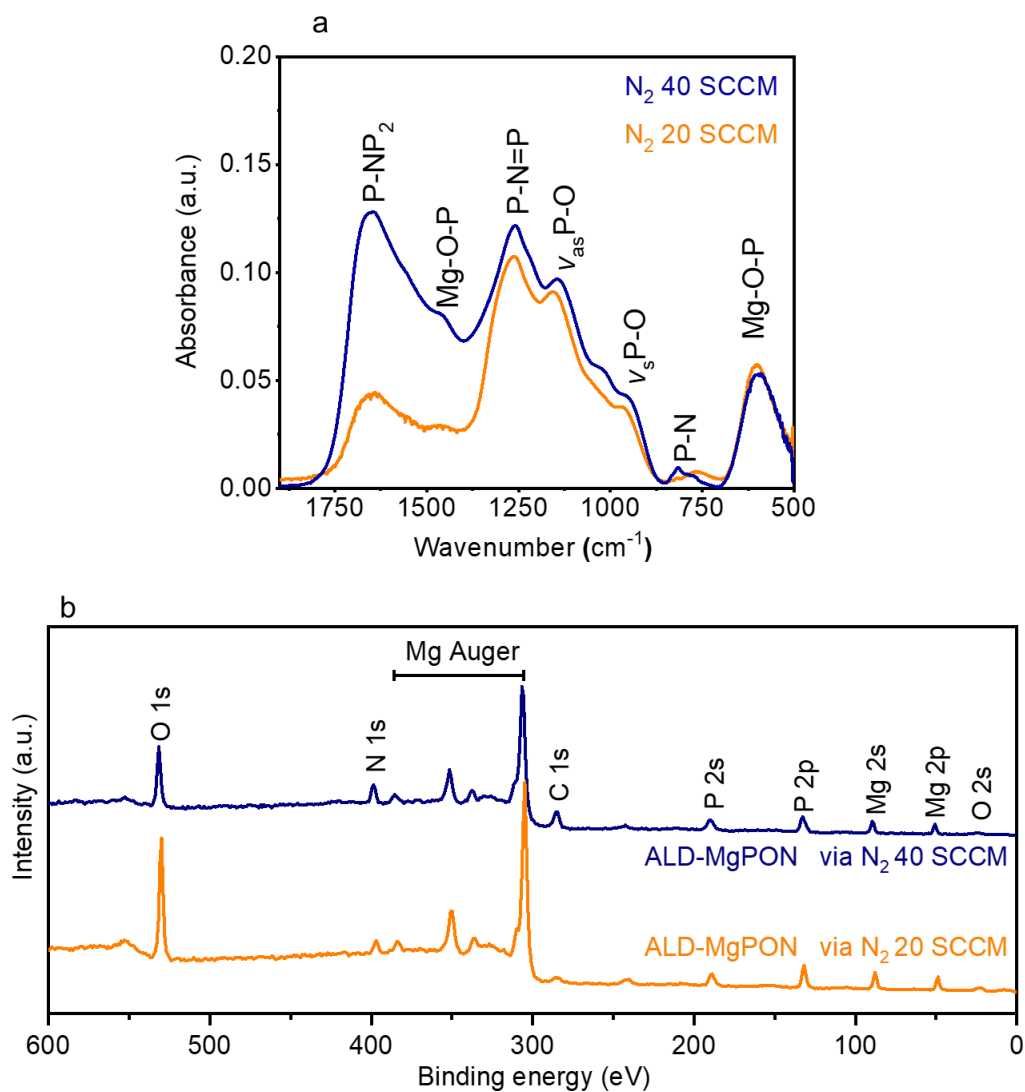


Figure S6. (a) FTIR and (b) Survey XPS spectra of ALD MgPON films deposited with N₂ flow rates of 20 and 40 SCCM.

Table S1. Atomic and relative elemental compositions of ALD MgPON films deposited with N₂ flow rates of 20 and 40 SCCM, which were calculated from the XPS survey spectra of Fig. S6b.

N ₂ flow rate (SCCM)	Atomic composition (%)				Relative composition
	Mg	P	O	N	
40	29.0	22.9	30.9	17.0	Mg _{1.3} P ₁ O _{1.3} N _{0.74}
20	29.1	19.7	43.3	7.9	Mg _{1.5} P ₁ O _{2.2} N _{0.40}

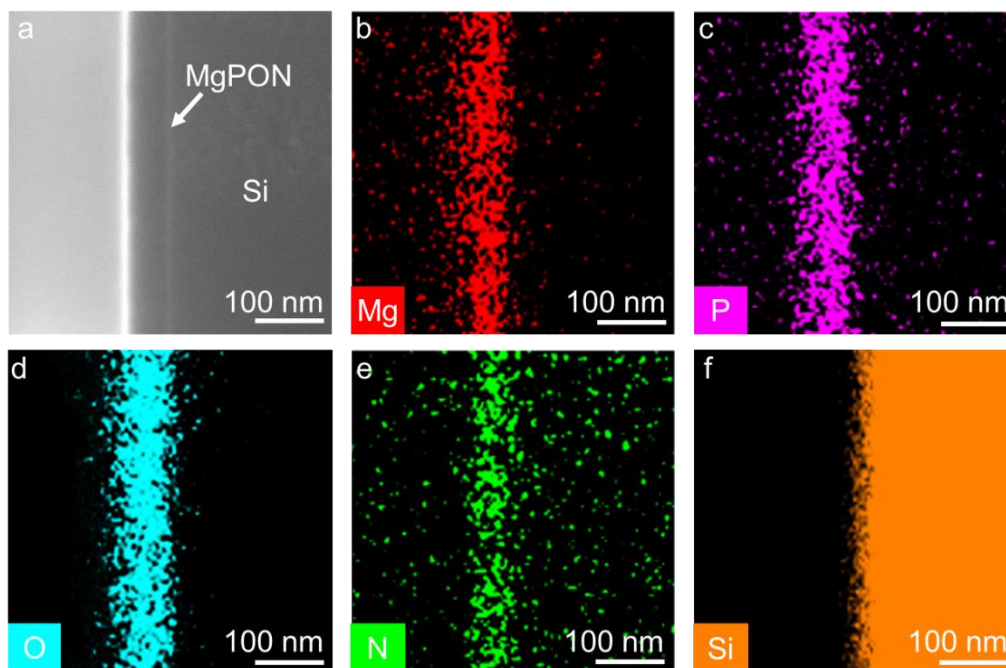


Figure S7. (a) Cross-sectional SEM image of an ALD MgPON SSE film deposited at 125 °C on the sidewall of the trench on a patterned Si substrate (as shown in Figure 4) and (b-f) the corresponding EDX mapping images for Mg, P, O, N, and Si.

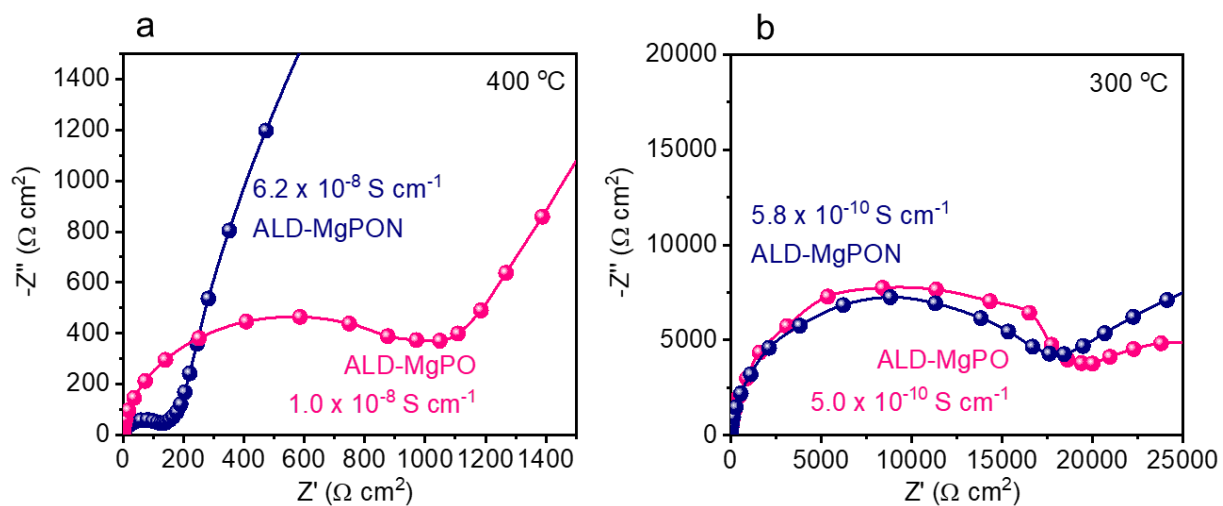


Figure S8. EIS curves of Pt/MgPON/Pt and Pt/MgPO/Pt symmetric cells measured at (a) 400 °C and (b) 300 °C.

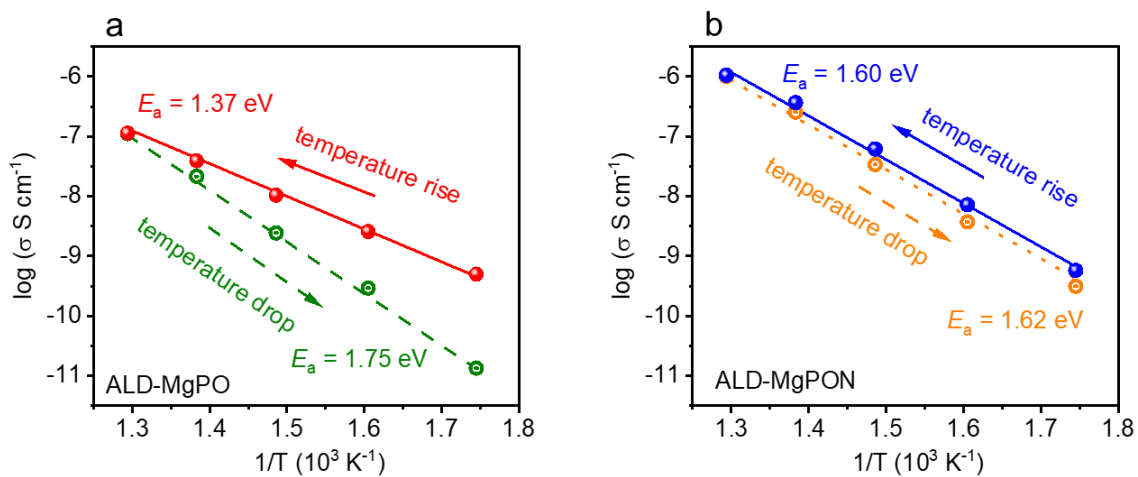


Figure S9. Arrhenius plots of the ionic conductivity of the (a) ALD MgPO and (b) MgPON SSE films, measured with an ambient temperature rise and drop cycle between 300 and 500 °C.

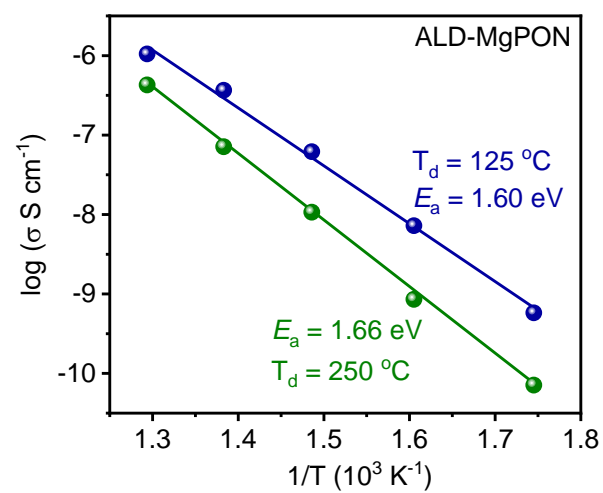


Figure S10. Arrhenius plots of the ionic conductivities measured from 300 to 500 °C for the ALD MgPON SSE films deposited at 125 and 250 °C.

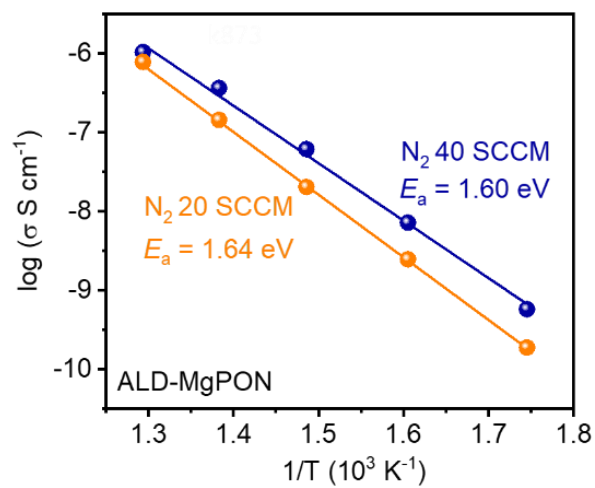


Figure S11. Arrhenius plots of the ionic conductivities measured from the ALD MgPON SSE films deposited with N₂ flow rates of 20 and 40 SCCM during the N₂ plasma process.